Brief Communication

MOLECULAR METABOLISM

Real-time monitoring of cAMP in brown adipocytes reveals differential compartmentation of β_1 and β_3-adrenoceptor signalling

Sukanya Arcot Kannabiran [1,2], Dominic Gosejacob [1,*], Birte Niemann [1,3], Viacheslav O. Nikolaev [4,], Alexander Pfeifer [1,2,3,***]**

ABSTRACT

Objective: 3′,5′-Cyclic adenosine monophosphate (cAMP) is a central second messenger governing brown adipocyte differentiation and function. β-adrenergic receptors (β-ARs) stimulate adenylate cyclases which produce cAMP. Moreover, cyclic nucleotide levels are tightly controlled by phosphodiesterases (PDEs), which can generate subcellular microdomains of cAMP. Since the spatio-temporal organisation of the cAMP signalling pathway in adipocytes is still unclear, we sought to monitor real-time cAMP dynamics by live cell imaging in pre-mature and mature brown adipocytes.

Methods: We measured the real-time dynamics of cAMP in murine pre-mature and mature brown adipocytes during stimulation of individual β-AR subtypes, as well as its regulation by PDEs using a Förster Resonance Energy Transfer based biosensor and pharmacological tools. We also correlated these data with β-AR stimulated lipolysis and analysed the expression of β-ARs and PDEs in brown adipocytes using qPCR and immunoblotting. Furthermore, subcellular distribution of PDEs was studied using cell fractionation and immunoblots.

Results: Using pre-mature and mature brown adipocytes isolated from transgenic mice expressing a highly sensitive cytosolic biosensor Epac1-camps, we established real-time measurements of cAMP responses. PDE4 turned out to be the major PDE regulating cytosolic cAMP in brown preadipocytes. Upon maturation, PDE3 gets upregulated and contributes with PDE4 to control β_1-AR-induced cAMP. Unexpectedly, β_3-AR initiated cAMP is resistant to increased PDE3 protein levels and simultaneously, the control of this microdomain by PDE4 is reduced upon brown adipocyte maturation. Therefore we postulate the existence of distinct cAMP pools in brown adipocytes. One cAMP pool is formed by β_1-AR associated with PDE3 and PDE4, while another pool is centred around β_3-AR and is much less controlled by these PDEs. Functionally, lower control of β_3-AR initiated cAMP by PDE3 and PDE4 facilitates brown adipocyte lipolysis, while lipolysis activated by β_1-AR and is under tight control of PDE3 and PDE4.

Conclusions: We have established a real-time live cell imaging approach to analyse brown adipocyte cAMP dynamics in real-time using a cAMP biosensor. We showed that during the differentiation from pre-mature to mature murine brown adipocytes, there was a change in PDE-dependent compartmentation of β_1-and β_3-AR-initiated cAMP responses by PDE3 and PDE4 regulating lipolysis.

Keywords Brown adipocytes; cAMP; PDE; FRET; Beta receptors; Compartmentation

1. INTRODUCTION

The thermogenic potential of brown adipose tissue (BAT) is the basis for its effect on whole-body energy expenditure and metabolism [1—4]. Since the identification of BAT in humans [1—5], it has been recognized as potential therapeutic target to combat obesity and related comorbidities, and attempts have been made to fully comprehend the biology of BAT.

BAT is physiologically activated by cold exposure, which induces the release of norepinephrine (NE) from the sympathetic nervous system [6]. The binding of NE to G-protein-coupled receptors (GPCRs) that are coupled to stimulatory G-proteins (G_s) activates adenylyl cyclases

[1]Institute of Pharmacology and Toxicology, University of Bonn, 53127, Bonn, Germany [2]Research Training Group 1873, University of Bonn, 53127, Bonn, Germany [3]Bonn International Graduate School of Drug Sciences (BIGS DrugS), Germany [4]Institute of Experimental Cardiovascular Research, University Medical Center Hamburg-Eppendorf, D-20246, Hamburg, Germany

*Corresponding author. E-mail: dominic.gosejacob@uni-bonn.de (D. Gosejacob).

**Corresponding author. E-mail: v.nikolaev@uke.de (V.O. Nikolaev).

***Corresponding author. Institute of Pharmacology and Toxicology, University of Bonn, 53127, Bonn, Germany. E-mail: alexander.pfeifer@uni-bonn.de (A. Pfeifer).

Received January 30, 2020 • Revision received March 23, 2020 • Accepted March 25, 2020 • Available online 1 April 2020

https://doi.org/10.1016/j.molmet.2020.100986

(ACs), increasing the intracellular concentration of the second messenger 3′,5′-cyclic adenosine monophosphate (cAMP) [7]. All three subtypes of G_s-coupled β-adrenergic receptors (β-ARs), β_1, β_2, and β_3, have been shown to be expressed in BAT [8,9], with β_3-AR being the most extensively studied receptor for stimulation of BAT in mice and humans. The major cAMP effector protein kinase A (PKA) [10,11] mediates activation of both adipose tissue triglyceride lipase [12] and hormone sensitive lipase [13] which break down storage lipids to free fatty acids. Free fatty acids bind to and activate the BAT-specific mitochondrial protein uncoupling protein-1 (UCP1), thereby increasing mitochondrial proton leak and converting the energy of substrate oxidation into heat [14].

The levels of cAMP are regulated not only via its synthesis by ACs but also at the level of its degradation by phosphodiesterases (PDEs) [15]. PDEs are intracellular enzymes which locally hydrolyse cAMP to adenosine monophosphate (AMP), thereby generating distinct subcellular cyclic nucleotide microdomains. They encompass 11 families of which PDE4, 7, and 8 are cAMP-specific; PDE5, 6, and 9 are 3′,5′-cyclic guanosine monophosphate (cGMP) specific; and PDE1, 2, 3, 10, and 11 are dual-specific PDEs which hydrolyse both cAMP and cGMP [16]. PDEs and their different isoforms have been described to regulate a vast range of functions in different organs [17—22].

The myriad of specific functions conveyed by the same second messenger can be achieved by intracellular compartmentation of cAMP in microdomains, which are associated with certain organelles or macromolecular protein complexes and are tightly regulated by local pools of PDEs [23]. To better understand compartmentalised cAMP signalling, Förster resonance energy transfer (FRET)-based imaging has been widely used as a tool to measure intracellular cAMP dynamics in real-time in a variety of cell types [24—26]. This is possible with FRET biosensors containing a single cAMP binding domain from the exchange protein directly regulated by cAMP (Epac) fused to a pair of fluorescent proteins, such as yellow fluorescent protein (YFP) and cyan fluorescent protein (CFP) [27].

Given the central role of cAMP in BAT activation, we set out to study its spatial and temporal organisation within brown adipocytes (BAs). Although the importance of compartmentalised β-AR-initiated cAMP signalling and its regulation by PDEs have been well-studied in cardiomyocytes and other cells [28—31], no reports are available on real-time cAMP measurements in BAs. Therefore we monitored real-time β-AR/cAMP dynamics in murine pre-mature and mature BAs and compared the role of PDEs in cAMP compartmentation between these cell types. We found that PDEs differentially compartmentalise β_1-and β_3-AR-initiated cAMP responses in murine pre-mature and mature BAs.

2. RESULTS

2.1. Real-time measurements of cAMP from different β-AR subtypes in murine brown adipocytes

To address the role of β-AR induced cAMP compartmentation, we first confirmed the mRNA expression of different β-AR receptors in transgenic Epac1-camps expressing pre-mature and mature BAs. As expected, β_1, β_2, β_3-ARs were expressed in both pre-mature and mature BAs (Suppl. Figure 1A-C). However, β_3-AR expression was low in pre-mature BAs, but strongly upregulated upon differentiation to mature BAs (Suppl. Figure 1C). We detected the mRNA and protein expression of cAMP-specific and dual-specific PDEs in murine pre-mature and mature BAs. qPCR and immunoblot analysis of the cAMP-specific PDEs PDE4A and PDE4B revealed their downregulation in mature BAs, albeit not significantly, while PDE4D was expressed similarly in both pre-mature and mature BAs (Suppl. Figure 2A, C, D, E). Amongst the dual-specific PDEs, PDE3A and PDE3B were upregulated on transcript and protein level in mature BAs while PDE2A was found in pre-mature and mature BAs (Suppl. Figure 2B, F, G, H). We also found the transcripts of PDE7A, PDE7B, PDE8A and PDE8B, while PDE4C was absent in both pre-mature and mature BAs among the cAMP-specific PDEs (Suppl. Figure 2A). Within the dual-specific PDEs, PDE1A, PDE2A, PDE3A, PDE3B, and PDE10A were expressed, while PDE1B and PDE11A were undetectable in pre-mature and mature BAs (Suppl. Figure 2B). We also detected expression of the PDEs of interest in this study in interscapular brown adipose tissue (iBAT), inguinal and gonadal white adipose tissue (iWAT and gWAT, respectively) using immunoblotting (Suppl. Figure 2C-H). PDE4A protein could be mainly detected in iBAT, while PDE4B and PDE4D were found in all adipose tissue depots. PDE2A, PDE3A and PDE3B were detected in all adipose tissue depots as well (Suppl. Figure 2F-H).

To determine the subcellular localisation of the PDEs, we performed fractionation of murine mature BA wherein we successfully isolated fractions of cytosol, endoplasmic reticulum (ER), and mitochondria and validated them with respective fraction-specific marker proteins (Suppl. Methods.1.3). Immunoblot analyses revealed that all the PDEs of interest, namely - PDE3A, 4A, 4B, 4D (Suppl. Figure 3A) and PDE2A (Suppl. Figure 3B) - are predominantly detected in the cytoplasm. PDE3B was restricted to ER membranes, while PDE3A was detected in ER membranes and the cytosol. We did not detect any of the PDEs in mitochondria. Apart from PDE3B, all analysed PDEs were detected in the cytosol. Therefore we decided to use a cytosolic version of the cAMP biosensor in the following experiments.

To study cAMP dynamics and compartmentation, we used FRET imaging in pre-mature and mature BAs. We isolated preadipocytes from BAT of new-born transgenic mice expressing the cytosolic cAMP sensor Epac1-camps. This biosensor allows the analysis of intracellular cAMP concentration by change of intramolecular FRET between CFP and YFP. FRET experiments employing Epac1-camps were performed on preadipocytes (Day 2) (Figure 1A,B) and in mature lipid-laden BA after differentiation (Day 7) (Figure 1C,D). Initially, we tested the FRET biosensor in adipocytes at both stages of differentiation by stimulating cAMP production with the β-AR agonist Isoproterenol (ISO, 100 nM) followed by addition of the unselective PDE inhibitor 3-isobutyl-1-methylxanthin (IBMX, 100 μM) plus the adenylyl cyclase activator Forskolin (Fsk, 10 μM) to elicit a maximal cAMP response. A clear increase of cAMP production reflected by a decrease of YFP/CFP ratio was detected in both pre-mature (Figure 1B) and mature BAs (Figure 1D).

We next performed FRET measurements using transgenic mice expressing Epac1-camps with the aim to establish the submaximal ligand concentrations which can be used to activate the different β-ARs to comparable amounts without saturating the biosensor response in pre-mature and mature BAs. We used ISO, a synthetic agonist for β-ARs; NE, a physiological agonist; and CL 316,243 (CL), a selective β_3-AR agonist, followed by the addition of IBMX and Fsk. The β-AR induced-Epac1-camps FRET responses were calculated in relation to R_0 and R_{max} and plotted as concentration-response curves (Figure 1E—G). For further experiments, we used concentrations of ligands based on the EC_{50} values calculated from the concentration-response curves (Figure 1E—G) for respective β-AR/cAMP responses as follows: 100 nM ISO, 100 nM NE and 50 μM CL in pre-mature BAs, and to 100 nM ISO, 500 nM NE and 10 μM CL in mature BAs.

To individually activate β_1-AR or β_2-AR, we selectively inhibited the respective β-AR subtype with β_2-blocker ICI 118551 (ICI, 50 nM) or β_1-AR blocker CGP 20712A (CGP, 100 nM) followed by addition of the

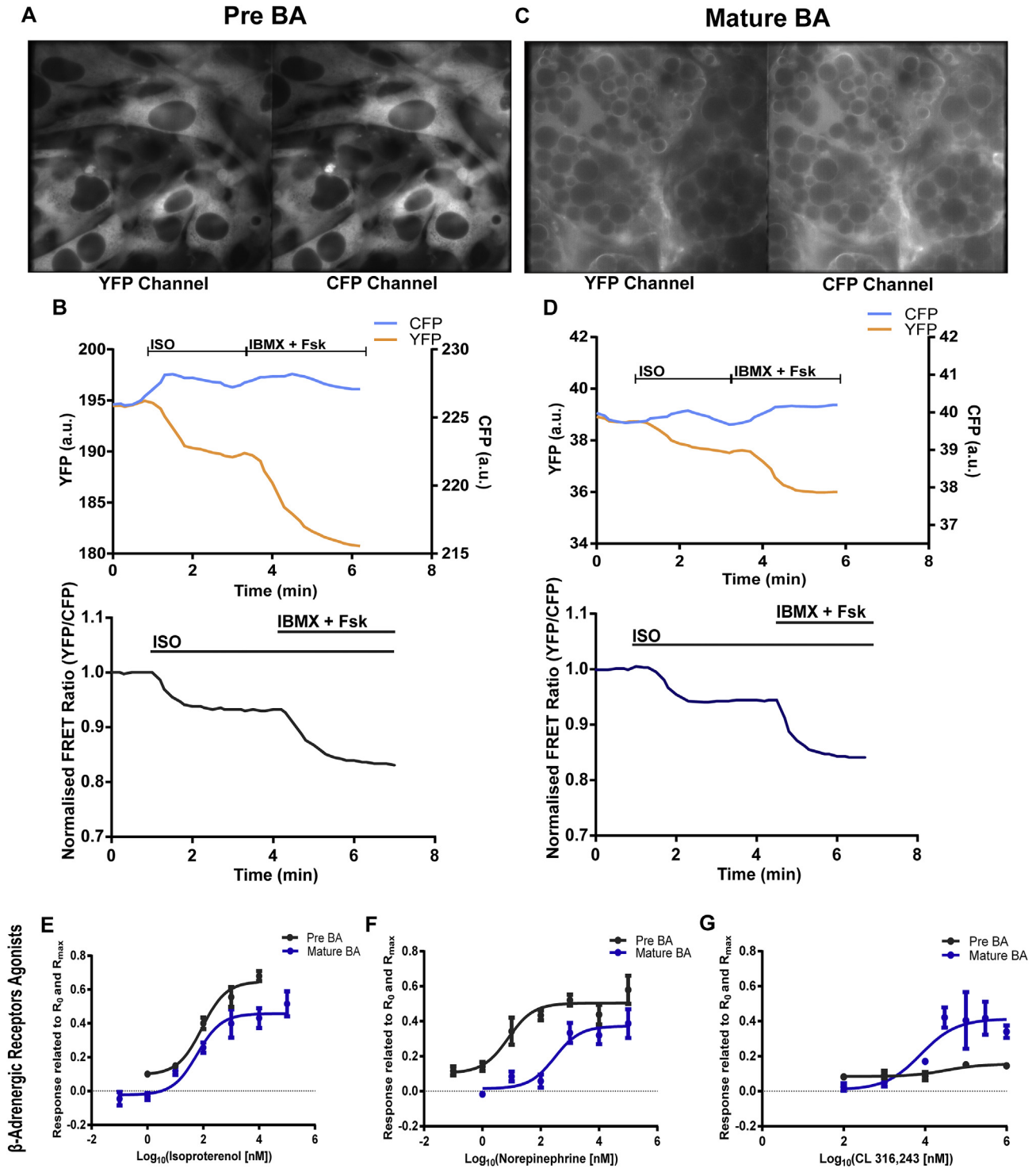

Figure 1: Measurement of real-time cAMP dynamics in pre-mature and mature murine transgenic brown adipocytes expressing Epac1-camps FRET biosensor. Single YFP and CFP channels from **(A)** pre-mature and **(C)** mature BAs expressing cytosolic FRET biosensor and their respective traces **(B)** and **(D)** followed by YFP/CFP ratio depicted as FRET traces upon stimulation with ISO (100 nM) and then by IBMX + Fsk (100 μM + 10 μM). A decrease in YFP/CFP ratio represents an increase of intracellular cAMP. **(E–G)** Concentration-response dependencies showing the differences in the amplitude of cAMP FRET responses induced by different β-AR ligands **(E)** Isoproterenol (ISO) (EC_{50}- 92.8 nM Pre-mature BAs, 60 nM mature BAs) **(F)** norepinephrine (NE) (EC_{50}- 7.7 nM Pre-mature BAs, 353.7 nM mature BAs) and **(D)** the β_3-AR agonist CL 316,243 (CL) (EC_{50}- 32.8 μM Pre-mature BAs, 7.8 μM mature BAs). FRET responses were normalized to basal corrected FRET ratio (R_0) and the maximal response evoked by IBMX + Fsk (R_{max}). n = 3-4, data are represented means ± S.E.M.

β-AR agonist ISO (100 nM), which has preferred binding affinity for $\beta_{1,2}$-AR compared to β_3-AR [32] (Suppl. Figure 4 A, B). To verify that ISO activates only β_1-and β_2-AR subtypes but not β_3-AR, we pre-incubated pre-mature and mature BAs with both ICI (50 nM) and CGP (100 nM) and found that this combination blocks the ISO-mediated cAMP increase in pre-mature and mature BA (Suppl. Figure 4 A, B). These data show the selectivity of ISO for β_1-and β_2-AR, but not β_3-AR. Similar results were obtained when cAMP was measured in mature BAs treated with ISO (10 nM) in combination with or without ICI (50 nM) and CGP (100 nM) using an Enzyme-linked Immunosorbent Assay (ELISA) (Suppl. Figure 4E). We also found that CL leads to a specific activation of β_3-AR because the β_3-AR induced cAMP increase in mature BA could not be blocked by the combination of ICI (50 nM) and CGP (100 nM) (Suppl. Figure 4C. We could stimulate cAMP specific to all three β-AR subtypes with the mentioned compounds in both pre-mature and mature BAs, respectively (Suppl. Figure 5A-G). Interestingly, even at high concentrations of all agonists, no full saturation of the sensor could be reached, suggesting that these cAMP responses are counterbalanced by activity of PDEs. Indeed, for example, when we applied the PDE4 inhibitor Rolipram to β_1-AR stimulated adipocytes, the response to this agonist increased dramatically from 43.4% ± 6.1 S.E.M to 78.2% ± 2.8 S.E.M in pre-mature BA and from 30.4% ± 5.8 S.E.M to 76.3% ± 2.8 S.E.M of the maximal response in mature BA, suggesting a tight control of β-AR initiated cAMP by PDE4. Therefore we next evaluated the role of individual PDE families in compartmentalisation of cAMP signals.

2.2. PDEs differently regulate cAMP responses in pre- and mature murine brown adipocytes upon β_1-AR activation

To address the hypothesis that PDE2, PDE3 and PDE4 may differentially control β-AR/cAMP dynamics in pre-mature and mature BAs, we performed real-time measurements of cAMP upon selective inhibition of these PDEs in context of individual receptor subtype stimulations. To activate β_1-AR, we selectively inhibited β_2-AR with the β_2-AR blocker, ICI (50 nM) followed by addition of the β-AR agonist ISO (100 nM). We recorded Epac1-camps FRET responses upon inhibition of different individual PDEs (PDE2 inhibitor, BAY 60-7550 100 nM, PDE3 inhibitor Cilostamide- 10 μM, PDE4 inhibitor Rolipram- 10 μM) followed by the unselective PDE inhibitor IBMX (100 μM) to elicit the maximum response (Figure 2A—F). The results revealed that in combination with β_1-AR stimulation in pre-BAs, PDE4 is the major PDE family regulating cAMP levels, since its inhibition contributed to a 1.8-fold ± 0.14 S.E.M (n = 6) and 3.5-fold ± 0.6 S.E.M (n = 6) stronger cAMP responses as compared to PDE3 and PDE2 inhibition, respectively. In contrast, in mature BAs, PDE3 and PDE4 contributed similarly as major regulators of cAMP levels, whereas PDE2 inhibitor responses were less pronounced (Figure 2G). The comparison of β_1-AR-induced cAMP production followed by PDE inhibition between pre-mature and mature BAs revealed that the inhibition of PDE3 induced significantly higher cAMP levels in the mature BAs compared to pre-mature BAs, while there was no difference in cAMP responses under PDE2 and PDE4 inhibition (Figure 2D). These data indicate that PDE4 is the major PDE controlling β_1-AR initiated cAMP in pre-mature and mature BAs. In contrast, PDE3 plays a major role in the control of β_1-AR initiated cAMP in mature but not pre-mature BAs.

2.3. PDEs similarly regulate cAMP production in pre-mature and mature murine brown adipocytes upon β_2-AR activation

Epac1-camps FRET responses were recorded by selectively activating β_2-AR. We inhibited β_1-AR with the β_1-AR blocker CGP 20712A (100 nM) followed by addition of ISO (100 nM) in pre-mature and mature BAs. FRET responses were recorded with the inhibition of different PDEs (PDE2 inhibitor, BAY 60-7550 100 nM, PDE3 inhibitor Cilostamide- 10 μM, PDE4 inhibitor Rolipram- 10 μM) followed by maximum stimulation with IBMX (100 μM) (Figure 3A—F). Under β_2-AR stimulation, in pre-mature BAs the effect of PDE4 inhibition was the highest in comparison to PDE2 and PDE3 inhibition, suggesting that PDE4 is the main regulator of cAMP production in pre-mature BAs. Interestingly, in mature BAs, the cAMP responses behaved similarly after inhibition of PDE2, PDE3 and PDE4. Overall, no significant difference in cAMP levels was observed with different PDE inhibitors between pre-mature and mature BAs (Figure 3G), suggesting degradation of β_2-AR initiated cAMP by PDEs is similarly controlled between pre-mature and mature BAs.

2.4. PDEs differently control β_3-AR-initiated cAMP in pre-mature and mature murine brown adipocytes

Finally, we selectively activated β_3-AR using its specific agonist CL in pre-mature (30 μM) and mature (50 μM) BAs followed by the addition of inhibitors for the different PDEs (PDE2 inhibitor, BAY 60-7550 100 nM, PDE3 inhibitor Cilostamide- 10 μM, PDE4 inhibitor Rolipram- 10 μM) and subsequent maximal stimulation of the cytosolic FRET sensor by IBMX (100 μM) (Figure 4A—F). We detected no differences in cAMP increase upon PDE2 and PDE3 inhibition between pre-mature and mature BAs (Figure 4G). PDE4 inhibition led to a stronger increase (2.3-fold ± 0.5 S.E.M, n = 6) of β_3-AR initiated cAMP in pre-mature BAs compared to mature BAs. This indicated that due to the low expression of β_3-AR in pre-mature BAs, PDE4 could have a stronger impact in restricting β_3-AR initiated cAMP in pre-mature BAs compared to mature BAs. From the increased expression of PDE3 in mature BAs, one would expect more PDE3-dependent-cAMP degradation. But unexpectedly, we did not detect a significant difference between the Cilostamide-induced effect after β_3-AR initiated activation of cAMP production in mature compared to pre-mature BA. This was in contrast to β_1-AR initiated cAMP, where the PDE3 effect was increased (Figure 4G). Thus PDE3 controls a loco-regional cAMP pool after stimulation with β_1-AR but not upon β_3-AR activation in mature BA. In pre-mature BA, the regulation of cAMP by PDEs was similarly dominated by PDE4 regardless of the stimulated β-ARs. Interestingly, we could recapitulate the main result that cAMP induced by β_3-AR stimulation is less controlled by PDEs compared to β_1-AR stimulation in murine mature BA using the cAMP ELISA Kit as a readout system (Suppl. Figure 6). We stimulated β_1-AR with ISO (10 nM) plus ICI (50 nM) pre-treatment or β_3-AR with CL (10 nM) in combination with PDE inhibitors. The PDE3 inhibitor Cilostamide (10 μM) did not lead to any further cAMP increase regardless if adipocytes were stimulated with β_1-or β_3-AR. In contrast, we detected a strong increase of cAMP upon Rolipram (10 μM) (PDE4 inhibitor) treatment when mature BAs were activated by β_1-AR, but not when they were activated with β_3-AR. This was in line with the real-time measurements of cAMP.

2.5. Role of PDE3/4 in β-AR initiated lipolysis in murine brown adipocytes

To test the functional relevance of our findings, we studied lipolysis as a readout for BA activation. We combined stimulation of BAs with either ISO (10 nM) to stimulate $\beta_{1/2}$-AR or CL (10 nM) to stimulate β_3-AR using values close to their EC_{50} [33] with inhibition of PDE3/4 and quantified lipolytic activity. Treatment with the $\beta_{1/2}$-AR agonist ISO-induced lipolysis, which was further amplified (2.0-fold ± 0.3 S.E.M, n = 6) by co-treatment with Cilostamide (10 μM) and Rolipram (10 μM), reaching a similar level as with co-treatment

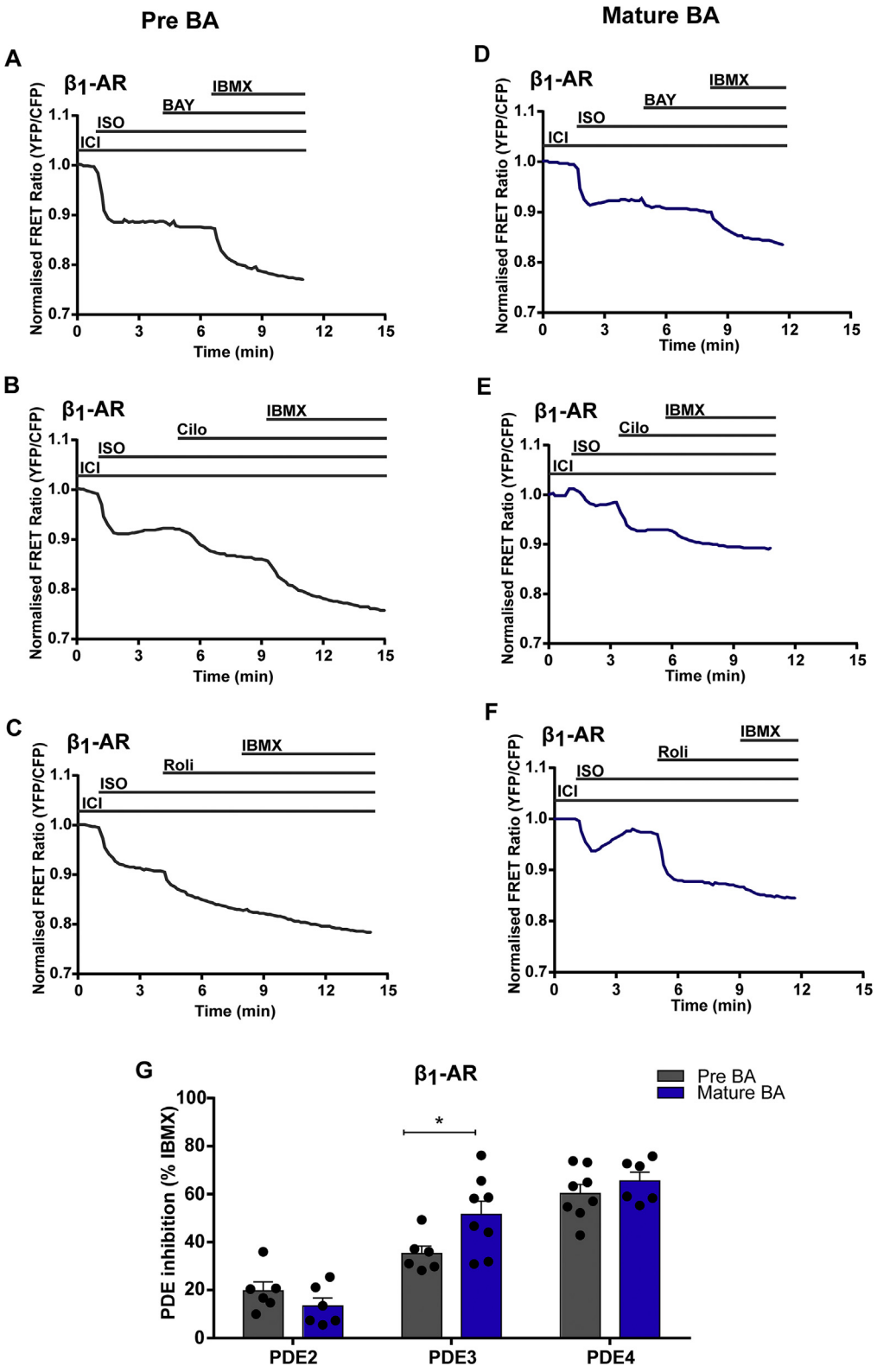

Figure 2: Differences in the regulation of cAMP dynamics by PDEs between pre-mature and mature murine transgenic brown adipocytes under β_1-AR activation. Representative FRET traces from cytosolic FRET sensor in pre-mature and mature BAs of β_1-AR activation by selectively blocking β_2-AR with 50 nM ICI 118551 and stimulation by 100 nM ISO followed by **(A, D)** PDE2 inhibitor BAY 60-7550 (BAY, 100 nM) **(B, E)** PDE3 inhibitor Cilostamide (Cilo, 10 μM) **(C, F)** PDE4 inhibitor Rolipram (Roli, 10 μM) with subsequent maximal FRET response achieved by inhibition of multiple PDEs with IBMX (100 μM). **(G)** Quantification of FRET responses to individual family-selective (PDE 2, 3 or 4) inhibitors upon β_1-AR stimulation are shown as a percentage of the maximal PDE inhibition obtained using the unselective inhibitor IBMX. n = 6-8. Bar graphs represent means ± S.E.M. Two-way ANOVA followed by Sidak's multiple comparison test was performed, significant differences correspond to *- $p < 0.05$.

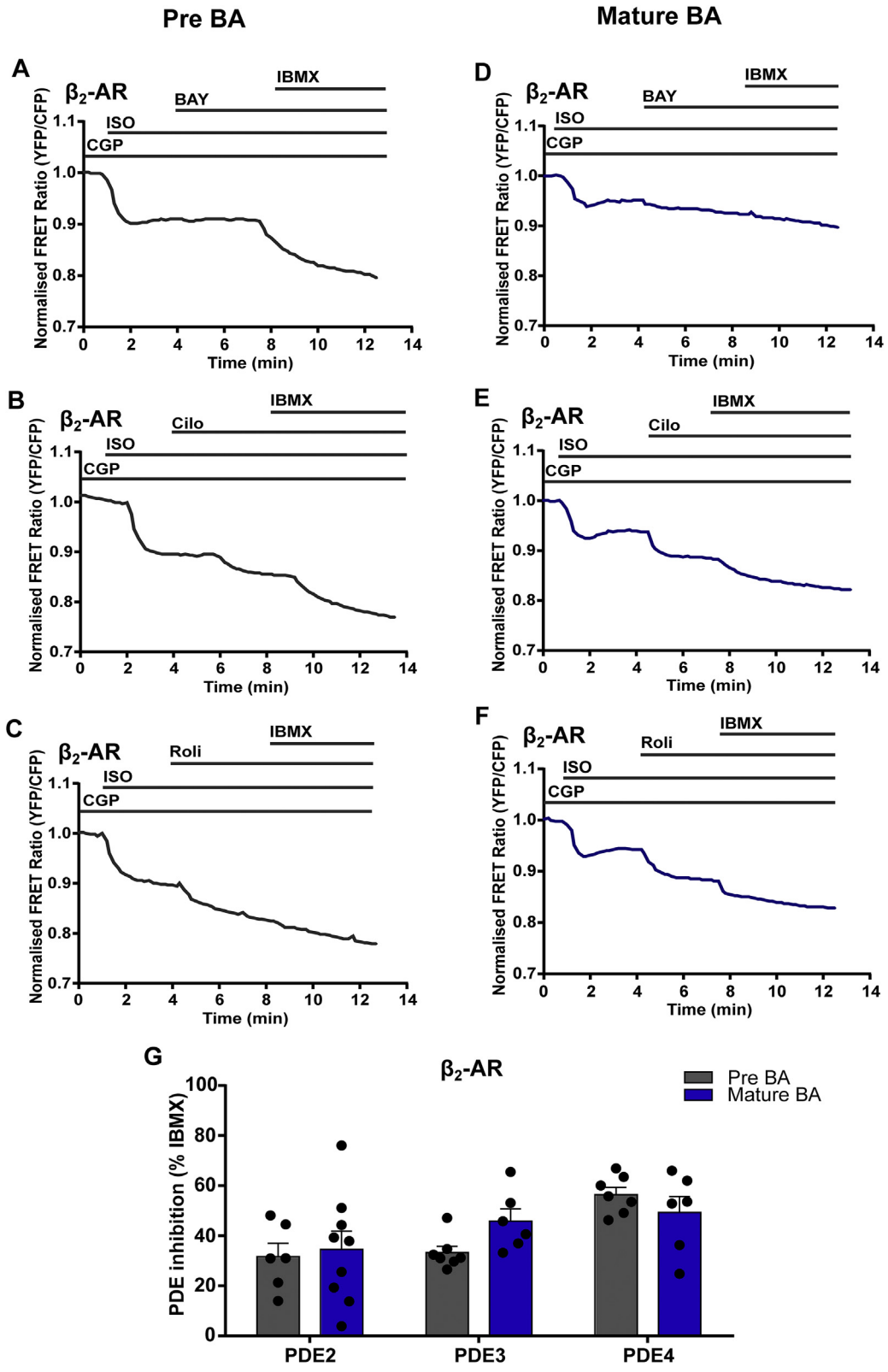

Figure 3: Regulation of cAMP dynamics by PDEs between pre-mature and mature murine transgenic brown adipocytes under β_2-AR activation. Representative FRET traces from cytosolic FRET sensor in pre-mature and mature BAs of β_2-AR activation by selectively blocking β_1-AR with 100 nM CGP 207102A and stimulation by 100 nM ISO followed by **(A, D)** PDE2 inhibitor BAY 60-7550 (BAY, 100 nM) **(B, E)** PDE3 inhibitor Cilostamide (Cilo, 10 μM) and **(C, F)** PDE4 inhibitor Rolipram (Roli, 10 μM) with subsequent maximal FRET response achieved by inhibition of multiple PDEs with IBMX (100 μM). **(G)** Quantification of FRET responses to individual family-selective (PDE 2, 3 or 4) inhibitors upon β_2-AR stimulation are shown as a percentage of the maximal PDE inhibition obtained using the unselective inhibitor IBMX. n = 6-9. Bar graphs represent means ± S.E.M. Two-way ANOVA followed by Sidak's multiple comparison test was performed.

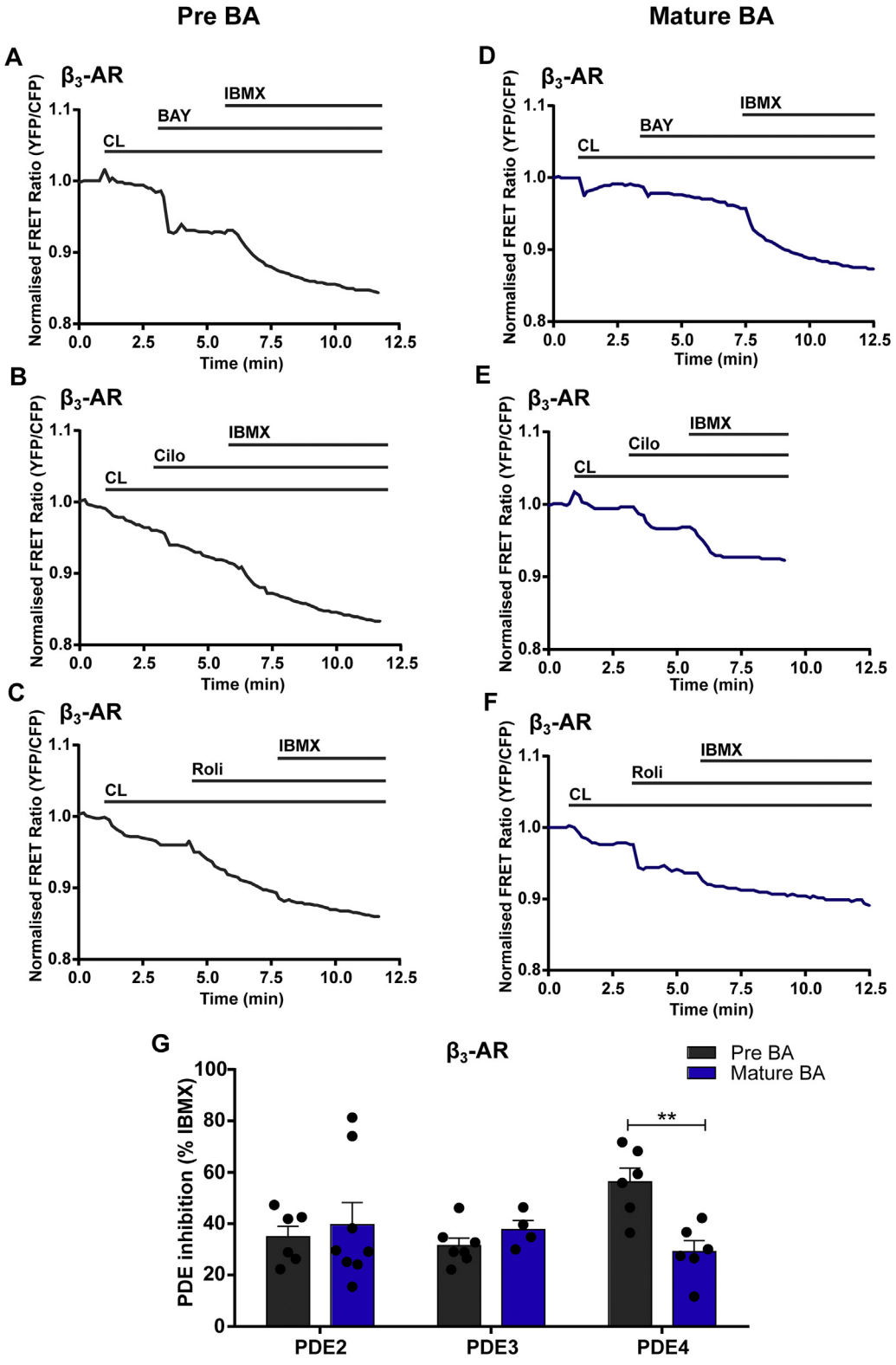

Figure 4: Differences in regulation of cAMP dynamics by PDEs between pre-mature and mature murine transgenic brown adipocytes under β_3-AR activation. Representative FRET traces from cytosolic FRET sensor in pre-mature and mature BAs of β_3-AR activation selectively stimulated with CL 316,243 (50 μM in pre-mature BAs, 10 μM in mature BAs) followed by **(A, D)** PDE2 inhibitor BAY 60-7550 (BAY, 100 nM) **(B, E)** PDE3 inhibitor Cilostamide (Cilo, 10 μM) **(C, F)** PDE4 inhibitor Rolipram (Roli, 10 μM) with subsequent maximal FRET response achieved by inhibition of PDEs by 100 μM IBMX. **(G)** Quantification of FRET responses to individual family-selective (PDE 2, 3 or 4) inhibitors upon β_3-AR stimulation are shown as a percentage of the maximal PDE inhibition obtained using the unselective inhibitor IBMX. n = 4-8. Bar graphs represent ± S.E.M. Two-way ANOVA followed by Sidak's multiple comparison test was performed, significant differences correspond to **- p = 0.01.

with the unselective PDE inhibitor IBMX (100 μM) (2.1-fold ± 0.3 S.E.M, n = 6) (Suppl. Figure 7). Interestingly, when BAs were stimulated with the selective β_3-AR agonist CL alone, lipolysis was induced to 1.5-fold ± 0.2 S.E.M (n = 6) higher as compared to Isoproterenol. Although the concentration of CL was close to the EC_{50} using lipolysis as readout [33,34], its response was not further increased by co-treatment with Cilostamide and Rolipram or IBMX (Suppl. Figure 7). This indicates that there are different cAMP pools related to the β_3-AR in brown adipocytes.

3. DISCUSSION

In BAs, the three different β-ARs co-exist but have different functions [8,9], giving rise to the idea of compartmentalised cAMP [9,34,35]. Measurement of intracellular cAMP by enzyme immunoassays have been successful, but this does not allow the analysis of distinct subcellular microdomains in real time. In contrast, FRET based biosensors enable such recordings which have been successfully used in other cellular systems, but have been so far lacking for primary adipocytes [23,27]. We therefore sought to establish live cell imaging of cAMP and to identify differences between individual β-AR induced pools of cAMP including their differential regulation by PDEs in two different stages of BA differentiation using FRET-based biosensors.

We confirmed the presence of cAMP and dual-specific PDEs, especially of PDE2, PDE3 and PDE4 families in murine pre-mature and mature BAs on mRNA level and protein level. Amongst the adipose tissue depots studied here, these PDEs and their isoforms were detected on protein level mainly in BAT and expression of these PDEs was confirmed also in both pre-mature and mature BA. We found an upregulation of PDE3A and PDE3B on transcript and protein level in mature BA. PDE3B plays an important role in mature adipocytes by inhibiting lipolysis and thereby enabling lipid accumulation upon adipocyte maturation [36–39]. We separated different cellular compartments of mature BAs and found PDE4A, PDE4B, PDE4D, PDE3A and PDE2A mainly in the cytosol as described for other cell types [16]. This led us to hypothesise the existence of multiple loco-regional cAMP pools within the cytosol regulated by different PDEs.

This study is the first to use a FRET biosensor as a tool to study the real-time dynamics of cAMP in BA. We optimized important parameters for our imaging system, namely as follows: exposure time and intensity of light source to excite the CFP donor and to avoid photobleaching that occurs due to covalent modification of fluorophores [27,40]. For pre-mature and mature BAs, an exposure time of 100 ms and 75% light intensity gave a good signal-to-noise ratio. We also realized that single cell measurements were not possible in pre-mature and mature BAs. Pre-mature BAs are grown in a dense monolayer to achieve efficient differentiation to mature BAs, as described previously [41]. Furthermore, the differentiation protocol used for our study gives rise to a layer of mature cells with dense multilocular lipid droplets. Therefore we chose a whole area of cells as region of interest (ROI) in both pre-mature and mature BAs for ratiometric analysis of YFP/CFP intensities.

A previous study demonstrated the general importance of PDE3/4 for the regulation of total cAMP levels in mature BAs [22]. In our study, we found that PDE3 and PDE4 tightly control β_1AR-induced cAMP signalling in pre-mature BAs, while in mature BAs, β_3-AR initiated cAMP is controlled equally but at a low level by all the three PDEs studied. We observed an upregulation of PDE3A and PDE3B in mature BAs. The increased regulation of β_1-AR initiated-cAMP by PDE3 in mature BAs in comparison to pre-mature BAs can be explained by the increase of PDE3 expression in mature BAs. However, this increase in PDE3 levels is not reflected by an increased inhibition of β_3-AR induced cAMP in mature compared to pre-mature BAs. This could possibly be due to a spatial separation of cAMP pools by the localisation of PDE3. We hypothesize that this separation might be established by signalosomes containing β_1-AR and PDE3A/B, while β_3-AR is part of a signalling complex or microdomain with low concentrations of PDE3 in mature BAs. The spatial separation of β_1-and β_3-receptor signalling could also be established on the subcellular level, because we and others found PDE3B in membrane compartments [16,39]. Although β_3-AR is lowly expressed in pre-mature BAs, we detected a high degree of PDE4 dependent regulation of β_3-AR cAMP pools in pre-mature BAs. Interestingly, the PDE4-dependent regulation is markedly reduced upon differentiation to mature BAs. This enables, together with increased β_3-AR expression, the β_3-receptor to generate higher amounts of local cAMP. Although we could not detect changes of PDE4 at the protein level, we postulate a redistribution of PDE4 isoforms between microdomains as shown for various PDEs in another cell type [42,43]. The cytosolic cAMP that we detected with this FRET sensor could be distinct from a membrane associated (e.g. ER or lipid droplet) cAMP pool. Functionally, we also observed that cAMP produced by the $\beta_{1/2}$- and β_3-AR both induce lipolysis in mature BAs. But $\beta_{1/2}$ -AR induced lipolysis was controlled more by PDE3/4 than β_3-AR induced lipolysis. Our data are also in good agreement with the importance of β_1-AR function in pre-mature BAs and the shift to predominant role of β_3-AR upon BA maturation [8,34]. The shift from β_1-AR signalling in pre-mature BAs to β_3-AR signalling in mature BAs is accompanied by an altered control of cAMP degradation by PDEs that allows cAMP signalling to adapt to an adipocyte-specific demand.

In summary, our study shows differences between pre-mature and mature BAs in terms of isoform-specific β-AR/cAMP compartmentation. It opens a possibility to understanding the different pools of β-AR initiated cAMP and their downstream signalling relevant for physiological regulation of pre-mature and mature BAs. How loco-regional cAMP is established in detail, which proteins are involved, and how β_3-AR dependent cAMP is degraded remain open questions and warrant further future investigations. The better understanding of these cAMP compartments might help to design novel pharmacological tools to modulate BA activity to tackle imbalances of energy homeostasis like obesity or cachexia.

4. METHODS

4.1. Isolation of murine primary brown adipocytes

iBAT isolated from new born pups of wildtype (WT) (C57BL/6J) and transgenic (TG) (FVB/N1) containing the Epac1-camps FRET sensor previously described [24]. These mice have been originally generated by pronuclear injection of a construct to ubiquitously express Epac1-camps sensor under the control of the CMV-enhancer chicken beta-actin (CAG) promotor [24]. The fat pads were minced finely in a digestion buffer (123 mM NaCl, 5 mM KCl, 1.3 mM $CaCl_2$, 5 mM Glucose, 100 mM HEPES) containing collagenase-type II (2 mg/mL, 1.5% fatty acid-free Bovine serum albumin (BSA), pH 7.4). The contents were shaken every 10 min in a shaker preheated to 37 °C at 120 RPM for 30 min until the fat pads were homogenised. The suspension was filtered through a 100 μM nylon mesh and allowed to stand on ice for 30 min. The middle layer containing mesenchymal stem cells (MSCs) from iBAT was filtered through a 30 μM nylon mesh and centrifuged at 700 g for 10 min. The pellets from 4 to 5 pups were combined, and resuspended in 5 mL of BAT culture medium (CM) (DMEM w/o pyruvate, 10% fetal bovine serum (FBS), 1% penicillin/streptomycin (P/S), 25 μg/mL sodium ascorbate, in mM — 10 HEPES,

0.004 Insulin, 0.004 Triiodothyronine (T3)) and 1 mL/well was seeded on a 6 well TC plate. This constituted a pool from one biological replicate and was considered as passage (P) 0. The cells were incubated overnight in the incubator at 37 °C, 5% CO_2. The next day, iBAT-MSCs were immortalised with lentiviral transduction of large T-antigen containing Simian virus 40 (SV40) (200 ng in 800 μL/6well) under phosphoglycerate kinase 1 (PKG) promoter in BAT CM. The following day, the well was filled with 3 mL BAT CM. 24 h post immortalisation, the medium was replaced by BA growth medium (GM) (DMEM without pyruvate, 10% FBS, 1% P/S) and the medium was changed every 2 days until the cells reached 90% confluency. After the cells reached 90% confluency, the cells were expanded and frozen in BA GM containing 10% DMSO for cryopreservation in −150 °C. These cells were used at passage (P) 4.

4.2. Culturing of murine primary brown adipocytes

One million cells from P4 were seeded in BA GM on a 6 well TC plate. The process of differentiation spans 11 days. 48 h post seeding (Day −2); BA GM was replaced by BA DM (DMEM w/o pyruvate, 10% FBS, 1% P/S, in nM- 20 Insulin, 1 T3). After Day −1, BA DM was replaced with BA induction medium (IM) (BA DM with in mM − 0.1 Dexamethasone, 0.5 IBMX). BA IM was changed to BA DM after 48 h and subsequently 2 more times. Depending on the need of the experiments, cells were harvested on Day −2 (pre-BA) and Day 7 (mature BA) of differentiation.

4.3. FRET measurements in murine brown adipocytes

For Epac1-camps based FRET measurements BAs were seeded onto round glass cover slides (Ø 25 mm) placed in a 6 well plate for measurement of pre-mature BAs and for mature BAs measurement. BAs were seeded on single well dishes (ibiTreat, μ-Dish$^{35mm,\ high}$) and were cultured as described (Results 4.2.). For respective measurements, DM was removed, cells were washed with FRET Buffer (in mM − NaCl 144, KCl 5.4, $MgCl_2 \cdot 6H_2O$ 1, $CaCl_2 \cdot 2H_2O$, 10 HEPES)− 400 μL (pre-BA) and 1 mL (mature BA) and loaded with the same amount of FRET buffer before starting the measurement. The compounds of interest were prepared in FRET buffer and concentration of compounds after each new subsequent addition was maintained to be the same.

We set up the FRET imaging system consisting of a light source (CoolLED p-100, 440 nM), inverted microscope (Leica DMI 4000 B, Leica), beam splitter (DualView) equipped with dcrx505 dichroic mirror, and ET480/40 plus ET535/30 emission filters (Chroma Technologies); along with a sCMOS camera (Photometrics) connected to a computer via an interface of Arduino UNO I/O switch board as described [23]. An oil immersion 40X objective was used. Post hardware configuration, software used was MicroManager 2.0 Beta coupled with Image J and the settings were as follows: Binning: 1*1, Preset: State 1. Prior to starting the experiments, a sharp image of the BAs was adjusted with the microscope and ROI covering both the images together from top to bottom; left and right from the channels were selected. An optimal signal-to-noise ratio for BAs was attained at every 10 s with an exposure time of 100 ms and 75% intensity from the LED light source. The CFP donor was excited at 440 nM. As the region of interest (ROI), we defined the whole area of confluent cell monolayers to quantify YFP and CFP signal intensities, because mature adipocytes can only be differentiated in confluent monolayers and cell boundaries cannot be detected without staining the plasma-membrane, using potentially interfering dyes. FRET traces for designed experiments were recorded when the FRET ratio attained a stable baseline. We determined the bleed through of the donor (CFP) into the acceptor (YFP) channel by transfecting HEK293 cells with the donor CFP sequence plasmid and the value for our system was 0.5. This value was subtracted from the FRET ratio and the calculations were performed as described [44].

4.4. Statistical anaylsis

The values of RT-PCR, the band density of immunoblots, and the FRET data were obtained from the software as described above. The results were analysed on Microsoft Excel 2016. The graphs and statistical analysis were performed on GraphPad Prism 6 software. Two-Way ANOVA followed by either Sidak, Tukey or Holm-Sidak's test statistical tests between different groups were used for multiple comparisons. Unpaired t-test was also used to analyse differences for biochemical experiments, as indicated in the figure legends.

4.5. Chemicals

Fsk, IBMX, and ISO were ordered from Sigma, BAY 60-7550. Cilostamide, was ordered from Cayman Chemicals. Rolipram, CGP20712 dihydrochloride, ICI 118551, and CL 316243 were ordered from Tocris.

AUTHOR CONTRIBUTIONS

S.A.K. designed and performed experiments, analysed data and wrote the manuscript. D.G. designed, performed experiments, analysed data, and wrote the manuscript. B.N. designed and performed experiments, analysed data. V.N., A.P. designed, supervised the experiments and wrote the manuscript.

ACKNOWLEDGMENTS

This work was funded by Deutsche Forschungsgemeinschaft (DFG, German Research Foundation) — 214362475/GRK1873/2 and Sonderforschungsbereich (SFB1328), project number 335447717/SFB1328, project A06 to VN and A09 AP. Additionally, we would like to thank Dr. Gabor Horvath from the Microscopy Core Facility at the Medical Faculty of University of Bonn for his advice.

CONFLICT OF INTEREST

The authors declare no conflict of interest.

APPENDIX A. SUPPLEMENTARY DATA

Supplementary data to this article can be found online at https://doi.org/10.1016/j.molmet.2020.100986.

REFERENCES

[1] Nedergaard, J., Bengtsson, T., Cannon, B., 2007. Unexpected evidence for active brown adipose tissue in adult humans. American Journal of Physiology. Endocrinology and Metabolism 293(2):E444−E452. https://doi.org/10.1152/ajpendo.00691.2006.

[2] Cypess, A.M., Lehman, S., Williams, G., Tal, I., Rodman, D., Goldfine, A.B., et al., 2009. Identification and importance of brown adipose tissue in adult humans. New England Journal of Medicine 360(15):1509−1517. https://doi.org/10.1056/NEJMoa0810780.

[3] Saito, M., Okamatsu-Ogura, Y., Matsushita, M., Watanabe, K., Yoneshiro, T., Nio-Kobayashi, J., et al., 2009. High incidence of metabolically active brown adipose tissue in healthy adult humans: effects of cold exposure and adiposity. Diabetes 58(7):1526−1531. https://doi.org/10.2337/db09-0530.

[4] Virtanen, K.A., Lidell, M.E., Orava, J., Heglind, M., Westergren, R., Niemi, T., et al., 2009. Functional brown adipose tissue in healthy adults. New England Journal of Medicine 360(15):1518—1525. https://doi.org/10.1056/NEJMoa0808949.

[5] van Marken Lichtenbelt, W.D., Vanhommerig, J.W., Smulders, N.M., Drossaerts, J.M., Kemerink, G.J., Bouvy, N.D., et al., 2009. Cold-activated brown adipose tissue in healthy men. New England Journal of Medicine 360(15):1500—1508. https://doi.org/10.1056/NEJMoa0808718.

[6] Prusiner, S.B., Cannon, B., Lindberg, O., 1968. Oxidative metabolism in cells isolated from brown adipose tissue. 1. Catecholamine and fatty acid stimulation of respiration. European Journal of Biochemistry 6(1):15—22. https://doi.org/10.1111/j.1432-1033.1968.tb00413.x.

[7] Reed, N., Fain, J.N., 1968. Stimulation of respiration in brown fat cells by epinephrine, dibutyryl-3',5'-adenosine monophosphate, and m-chloro(carbonyl cyanide)phenylhydrazone. Journal of Biological Chemistry 243(11):2843—2848.

[8] Bronnikov, G., Houstek, J., Nedergaard, J., 1992. Beta-adrenergic, cAMP-mediated stimulation of proliferation of brown fat cells in primary culture. Mediation via beta 1 but not via beta 3 adrenoceptors. Journal of Biological Chemistry 267(3):2006—2013.

[9] Collins, S., Daniel, K.W., Rohlfs, E.M., Ramkumar, V., Taylor, I.L., Gettys, T.W., 1994. Impaired expression and functional activity of the beta 3- and beta 1-adrenergic receptors in adipose tissue of congenitally obese (C57BL/6J ob/ob) mice. Molecular Endocrinology 8(4):518—527. https://doi.org/10.1210/mend.8.4.7914350.

[10] MacDonald, J.A., Storey, K.B., 1998. cAMP-dependent protein kinase from brown adipose tissue: temperature effects on kinetic properties and enzyme role in hibernating ground squirrels. Journal of Comparative Physiology B 168(7):513—525. https://doi.org/10.1007/s003600050172.

[11] Fredriksson, J.M., Thonberg, H., Ohlson, K.B., Ohba, K., Cannon, B., Nedergaard, J., 2001. Analysis of inhibition by H89 of UCP1 gene expression and thermogenesis indicates protein kinase A mediation of beta(3)-adrenergic signalling rather than beta(3)-adrenoceptor antagonism by H89. Biochimica et Biophysica Acta 1538(2—3):206—217. https://doi.org/10.1016/s0167-4889(01)00070-2.

[12] Schreiber, R., Diwoky, C., Schoiswohl, G., Feiler, U., Wongsiriroj, N., Abdellatif, M., et al., 2017. Cold-induced thermogenesis depends on ATGL-mediated lipolysis in cardiac muscle, but not Brown adipose tissue. Cell Metabolism 26(5):753—763. https://doi.org/10.1016/j.cmet.2017.09.004 e7.

[13] Holm, C., Fredrikson, G., Cannon, B., Belfrage, P., 1987. Hormone-sensitive lipase in brown adipose tissue: identification and effect of cold exposure. Bioscience Reports 7(11):897—904. https://doi.org/10.1007/bf01119481.

[14] Nicholls, D.G., Locke, R.M., 1984. Thermogenic mechanisms in brown fat. Physiological Reviews 64(1):1—64. https://doi.org/10.1152/physrev.1984.64.1.1.

[15] Butcher, R.W., Sutherland, E.W., 1962. Adenosine 3',5'-phosphate in biological materials. I. Purification and properties of cyclic 3',5'-nucleotide phosphodiesterase and use of this enzyme to characterize adenosine 3',5'-phosphate in human urine. Journal of Biological Chemistry 237:1244—1250.

[16] Bender, A.T., Beavo, J.A., 2006. Cyclic nucleotide phosphodiesterases: molecular regulation to clinical use. Pharmacological Reviews 58(3):488—520. https://doi.org/10.1124/pr.58.3.5.

[17] Wechsler, J., Choi, Y.-H., Krall, J., Ahmad, F., Manganiello, V.C., Movsesian, M.A., 2002. Isoforms of cyclic nucleotide phosphodiesterase PDE3A in cardiac myocytes. Journal of Biological Chemistry 277(41):38072—38078. https://doi.org/10.1074/jbc.M203647200.

[18] Rybalkin, S.D., Yan, C., Bornfeldt, K.E., Beavo, J.A., 2003. Cyclic GMP phosphodiesterases and regulation of smooth muscle function. Circulation Research 93(4):280—291. https://doi.org/10.1161/01.RES.0000087541.15600.2B.

[19] Netherton, S.J., Jimmo, S.L., Palmer, D., Tilley, D.G., Dunkerley, H.A., Raymond, D.R., et al., 2002. Altered phosphodiesterase 3-mediated cAMP hydrolysis contributes to a hypermotile phenotype in obese JCR:LA-cp rat aortic vascular smooth muscle cells: implications for diabetes-associated cardiovascular disease. Diabetes 51(4):1194—1200. https://doi.org/10.2337/diabetes.51.4.1194.

[20] Monterisi, S., Lobo, M.J., Livie, C., Castle, J.C., Weinberger, M., Baillie, G., et al., 2017. PDE2A2 regulates mitochondria morphology and apoptotic cell death via local modulation of cAMP/PKA signalling. Elife 6. https://doi.org/10.7554/eLife.21374.

[21] Beierwaltes, W.H., 2006. cGMP stimulates renin secretion in vivo by inhibiting phosphodiesterase-3. American Journal of Physiology - Renal Physiology 290(6):F1376—F1381. https://doi.org/10.1152/ajprenal.00209.2005.

[22] Kraynik, S.M., Miyaoka, R.S., Beavo, J.A., 2013. PDE3 and PDE4 isozyme-selective inhibitors are both required for synergistic activation of brown adipose tissue. Molecular Pharmacology 83(6):1155—1165. https://doi.org/10.1124/mol.112.084145.

[23] Herget, S., Lohse, M.J., Nikolaev, V.O., 2008. Real-time monitoring of phosphodiesterase inhibition in intact cells. Cellular Signalling 20(8):1423—1431. https://doi.org/10.1016/j.cellsig.2008.03.011.

[24] Calebiro, D., Nikolaev, V.O., Gagliani, M.C., Filippis, T., de Dees, C., Tacchetti, C., et al., 2009. Persistent cAMP-signals triggered by internalized G-protein-coupled receptors. PLoS Biology 7(8):e1000172. https://doi.org/10.1371/journal.pbio.1000172.

[25] Werthmann, R.C., Hayn, K., von Nikolaev, V.O., Lohse, M.J., Bunemann, M., 2009. Real-time monitoring of cAMP levels in living endothelial cells: thrombin transiently inhibits adenylyl cyclase 6. The Journal of Physiology 587(Pt 16):4091—4104. https://doi.org/10.1113/jphysiol.2009.172957.

[26] Mironov, S.L., Skorova, E., Taschenberger, G., Hartelt, N., Nikolaev, V.O., Lohse, M.J., et al., 2009. Imaging cytoplasmic cAMP in mouse brainstem neurons. BMC Neuroscience 10:29. https://doi.org/10.1186/1471-2202-10-29.

[27] Borner, S., Schwede, F., Schlipp, A., Berisha, F., Calebiro, D., Lohse, M.J., et al., 2011. FRET measurements of intracellular cAMP concentrations and cAMP analog permeability in intact cells. Nature Protocols 6(4):427—438. https://doi.org/10.1038/nprot.2010.198.

[28] Nikolaev, V.O., Bunemann, M., Schmitteckert, E., Lohse, M.J., Engelhardt, S., 2006. Cyclic AMP imaging in adult cardiac myocytes reveals far-reaching beta1-adrenergic but locally confined beta2-adrenergic receptor-mediated signaling. Circulation Research 99(10):1084—1091. https://doi.org/10.1161/01.RES.0000250046.69918.d5.

[29] Nikolaev, V.O., Moshkov, A., Lyon, A.R., Miragoli, M., Novak, P., Paur, H., et al., 2010. Beta2-adrenergic receptor redistribution in heart failure changes cAMP compartmentation. Science 327(5973):1653—1657. https://doi.org/10.1126/science.1185988.

[30] Mika, D., Richter, W., Westenbroek, R.E., Catterall, W.A., Conti, M., 2014. PDE4B mediates local feedback regulation of beta(1)-adrenergic cAMP signaling in a sarcolemmal compartment of cardiac myocytes. Journal of Cell Science 127(Pt 5):1033—1042. https://doi.org/10.1242/jcs.140251.

[31] Wright, P.T., Bhogal, N.K., Diakonov, I., Pannell, L.M.K., Perera, R.K., Bork, N.I., et al., 2018. Cardiomyocyte membrane structure and cAMP compartmentation produce anatomical variation in beta2AR-cAMP responsiveness in murine hearts. Cell Reports 23(2):459—469. https://doi.org/10.1016/j.celrep.2018.03.053.

[32] Hoffmann, C., Leitz, M.R., Oberdorf-Maass, S., Lohse, M.J., Klotz, K.-N., 2004. Comparative pharmacology of human beta-adrenergic receptor subtypes–characterization of stably transfected receptors in CHO cells. Naunyn-Schmiedeberg's Archives of Pharmacology 369(2):151—159. https://doi.org/10.1007/s00210-003-0860-y.

[33] Atgie, C., D'Allaire, F., Bukowiecki, L.J., 1997. Role of beta1- and beta3-adrenoceptors in the regulation of lipolysis and thermogenesis in rat brown

adipocytes. American Journal of Physiology 273(4):C1136–C1142. https://doi.org/10.1152/ajpcell.1997.273.4.C1136.

[34] Cannon, B., Nedergaard, J., 2004. Brown adipose tissue: function and physiological significance. Physiological Reviews 84(1):277–359. https://doi.org/10.1152/physrev.00015.2003.

[35] Zhao, J., Cannon, B., Nedergaard, J., 1997. alpha1-Adrenergic stimulation potentiates the thermogenic action of beta3-adrenoreceptor-generated cAMP in brown fat cells. Journal of Biological Chemistry 272(52):32847–32856. https://doi.org/10.1074/jbc.272.52.32847.

[36] Czech, M.P., Tencerova, M., Pedersen, D.J., Aouadi, M., 2013. Insulin signalling mechanisms for triacylglycerol storage. Diabetologia 56(5):949–964. https://doi.org/10.1007/s00125-013-2869-1.

[37] Arner, P., Langin, D., 2014. Lipolysis in lipid turnover, cancer cachexia, and obesity-induced insulin resistance. Trends in Endocrinology and Metabolism 25(5):255–262. https://doi.org/10.1016/j.tem.2014.03.002.

[38] Fruhbeck, G., Mendez-Gimenez, L., Fernandez-Formoso, J.-A., Fernandez, S., Rodriguez, A., 2014. Regulation of adipocyte lipolysis. Nutrition Research Reviews 27(1):63–93. https://doi.org/10.1017/S095442241400002X.

[39] DiPilato, L.M., Ahmad, F., Harms, M., Seale, P., Manganiello, V., Birnbaum, M.J., 2015. The role of PDE3B phosphorylation in the inhibition of lipolysis by insulin. Molecular and Cellular Biology 35(16):2752–2760. https://doi.org/10.1128/MCB.00422-15.

[40] Zal, T., Gascoigne, N.R.J., 2004. Photobleaching-corrected FRET efficiency imaging of live cells. Biophysical Journal 86(6):3923–3939. https://doi.org/10.1529/biophysj.103.022087.

[41] Jennissen, K., Haas, B., Mitschke, M.M., Siegel, F., Pfeifer, A., 2013. Analysis of cGMP signaling in adipocytes. Methods in Molecular Biology 1020:175–192. https://doi.org/10.1007/978-1-62703-459-3_11.

[42] Sprenger, J.U., Perera, R.K., Steinbrecher, J.H., Lehnart, S.E., Maier, L.S., Hasenfuss, G., et al., 2015. In vivo model with targeted cAMP biosensor reveals changes in receptor-microdomain communication in cardiac disease. Nature Communications 6:6965. https://doi.org/10.1038/ncomms7965.

[43] Perera, R.K., Sprenger, J.U., Steinbrecher, J.H., Hubscher, D., Lehnart, S.E., Abesser, M., et al., 2015. Microdomain switch of cGMP-regulated phosphodiesterases leads to ANP-induced augmentation of beta-adrenoceptor-stimulated contractility in early cardiac hypertrophy. Circulation Research 116(8):1304–1311. https://doi.org/10.1161/CIRCRESAHA.116.306082.

[44] Kraft, A.E., Nikolaev, V.O., 2017. FRET microscopy for real-time visualization of second messengers in living cells. Methods in Molecular Biology 1563:85–90. https://doi.org/10.1007/978-1-4939-6810-7_6.

